Elucidating Chemical and Morphological Changes in Tetrachloroauric Solutions Induced by X-ray Photochemical Reaction

Qing Ma,*,† Ralu Divan,‡ Derrick C. Mancini,‡ and Denis T. Keane†

DuPont−Northwestern−Dow Collaborative Access Team (DND-CAT), Northwestern University Synchrotron Research Center, 9700 South Cass Avenue, Argonne, IL 60439 and Center for Nanoscale Materials, Argonne National Laboratory, 9700 South Cass Avenue, Argonne, IL 60439

Received: October 30, 2007; Revised Manuscript Received: February 11, 2008

Chemical and morphological changes induced by an X-ray photochemical reaction in tetrachloroauric solutions leading to Au^{3+}-to-Au^0 reduction are monitored in real time by X-ray absorption spectroscopy and X-ray small angle scattering. Prior to metal precipitation, the intermediate state, also observed by other techniques, is unambiguously determined for the first time to be the reduction of Au^{3+} to Au^{1+}, whose kinetics is strictly of the zeroth order. The morphological changes occur simultaneously in the solutions, that is, the gold complexes rearrange and aggregate, as unequivocally observed by the correlated changes in the Au L_3 emission and small angle scattering intensities. The experimental evidence indicates that the eventual metal precipitation is strongly influenced by the changing solution acidity under X-ray irradiation. Detailed local structure changes are also described.

Introduction

One of the important aspects for tailoring nanostructure formation in solutions is to understand the reaction mechanism, including the details about the intermediates generated in the reactions.[1,2] Tetrachloroauric ($AuCl_4^-$) solutions are broadly used to produce gold nanoparticles chemically,[3,4] thermally,[5] or photochemically[6] for applications in efficient catalysts, advanced electronics, and medical diagnoses. Despite numerous studies of particle synthesis and production,[1,2] few studies were carried out to elucidate the evolution in the solutions prior to particle formation. Knowledge of the details of intermediates and the interaction between gold complexes prior to particle formation is critical for controlling the sizes, shapes, and thus the properties of the nanoparticles.[1,2,7,8]

In his potentiometric titration experiments of $AuCl_4^-$ solutions, more than half a century ago, Bjerrum observed an increase, instead of the normally expected decrease, in the electrochemical potential at the onset of the titration process.[9] This was confirmed by Lingane a decade later.[10] This increase was attributed to the reduction of $AuCl_4^-$ to $AuCl_2^-$ as an intermediate state towards metal precipitation. In the UV- or γ-ray-induced reduction experiments, initial irradiation does not produce any particles detectable by the optical spectrometer, while the optical band associated with $AuCl_4^-$ decreases and the solutions become discolored. Henglein has suggested that this is due to a lower valence state being produced and reasoned that it is likely to be Au^{1+} because it has a longer lifetime than Au^{2+}.[11] Gachard et al. used the Au^{1+} assumption in their mechanism discussion in their γ-ray irradiation work.[12]

In an attempt to confirm this spectroscopically, two recent Raman studies contradicted each other due to ambiguity in the data interpretation.[13,14] Subsequent X-ray absorption studies supported one of these results that negated the existence of $AuCl_2^-$ during thermal reduction.[15] In studying linear $AuCl_2^-$ ions in CH_3CN using optical spectroscopy, Koutek and Mason assigned a weak band (parity forbidden d → s transitions) and an intense band (parity allowed d → p transitions) to these ions.[16] However, both the band positions and shapes depend on the solvents.[17,11] The bands, if existing, are overshadowed in the presence of $AuCl_4^-$ ions, and no attempts have been reported to differentiate them. In addition, the questions have rarely been tackled regarding what kinetics this intermediate state follows, when produced, and what the morphological consequences are as it forms in the solutions.

In this paper, we address these issues using X-ray absorption spectroscopy (XAS) and small angle X-ray scattering (SAXS) simultaneously, which allows the study of chemical and morphological changes in the solutions.[18,19] Chemical reactions are induced by synchrotron X-ray photons. The kinetics of chemical reaction in the solutions that leads to the Au^{3+}-to-Au^0 reduction is followed in real time.

Experimental Methods

X-ray experiments were carried out at the bending magnet beamline (5-BM-D), operated by DND-CAT, at the Advanced Photon Source. The beamline uses a Si(111) monochromator for energy selection. The energy resolution at the Au L_3 edge (11918.7 eV) is ~1.4 eV. The synchrotron storage ring was operated in the "top-up" mode with the electron beam current kept at ~100 mA. The incident X-ray flux density at the sample is estimated to be 8×10^9 s^{-1} mm^{-2}. The X-ray beam size in the experimental station is selected by two sets of Huber slits, which is either 1×1 mm^2 or 1×8 mm^2. Therefore, the X-ray deposit rate is 15 μW or 120 μW. The solutions (0.4−2 mM) were prepared by dissolving hydrated tetrachloroauric acid ($HAuCl_4 \cdot 4H_2O$) in deionized water. The pH values are from 2.8 for the 2 mM solution to 3.5 for the 0.8 mM solution (ORION-290A). A buffered $HAuCl_4$ solution with pH = 2.8 is also prepared using 100 mL 0.1 M $KC_8H_5O_4$ and 57.8 mL 0.1 M HCl for comparison.

* Corresponding author E-mail: q-ma@northwestern.edu. Phone: 630-252-03229. Fax: 630-252-0226.
† DND-CAT.
‡ Argonne National Laboratory.

10.1021/jp7104852 CCC: $40.75
Published on Web 04/24/2008

The incident X-ray intensity is measured by an ion chamber (Oxford Danfysik). A 13-element Ge solid state detector (Canberra) was used to collect the Au L_3 fluorescence emission for X-ray absorption near edge structure (XANES) and extended X-ray absorption fine structure (EXAFS) spectra. The Fourier transform of the EXAFS spectrum reveals the inter-atomic distances and coordination numbers around Au atoms.[18] The detector has an energy resolution of ~2% or ~250 eV at the Au L_3 absorption edge, which is sufficient to collect the Au L_3 fluorescence emission (at ~9700 eV) with little background. A MAR 165 (Mar USA) wide area detector was used for small angle X-ray scattering. A Tungsten beam stop of 5 mm in diameter is used to block the direct beam, from which the X-ray induced current is measured through a SR570 amplifier to determine the sample absorbance. The air scattering is minimized by placing a vacuumed flight pipe between the sample and the MAR 165 area detector. The scattering in the q range from 0.005 to 0.2 $Å^{-1}$ is measured. The solution samples are held in Kapton-sealed polypropylene or Kapton-insulated and -sealed Al cells. For XAS measurements, the incident beam size is 1 × 8 mm^2, for which ~0.4 cc solutions are used in the 8 × 15 × 3.5 cm^3 cell. For simultaneous XAS and SAXS measurements, the beam size is 1 × 1 mm^2, for which ~0.05 cc solutions are used in the 6 mm-diameter and 2 mm-thick cell. For all measurements, the sample is placed 45° both to the incident X-ray beam and to the Ge detector, which are perpendicular to each other. This introduces a negligible error in the SAXS angle calculation.

Results and Discussion

Under thermal or chemical treatment or light irradiation, the $AuCl_4^-$ aqueous solutions undergo reduction reaction and generate nanoparticles.[3–6] The cause of the reduction detailed for γ-ray irradiation should readily apply to X-ray irradiation.[20,21] In brief, high energy X-ray photons generate strong reducing agents, such as hydrated electrons,[22] in aqueous solutions that undergo chemical reactions, such as $Au^{3+} + 3e_{eq}^- \rightarrow Au$. The gold deposits on the Kapton windows are the end products.

A. Chemical Changes in the Aqueous Solutions under X-ray Irradiation. Figure 1 illustrates the X-ray-induced gold reduction kinetics by the integrated Au L_3 fluorescence emission intensity for three $HAuCl_4^-$ solutions (see Supporting Information). Note that the time is plotted logarithmically to make room for the inset. The time resolution is ~5 min, which is adequate for the slow kinetics shown here. The kinetics is essentially very similar to γ-ray-induced gold reduction, reported by Gachard et al. using the optical spectroscopy technique.[12] The zero amplitude in Figure 1 is obtained after subtracting out the emission intensity at the time "zero". There are three distinct regions. The first region is before any significant increases in the Au L_3 emission intensity. The second region includes the linear rise in the magnitude, and the third region is the plateau. Unlike the optical data, however, the data in Figure 1 also carry the information on the evolution prior to metal precipitation, such as the initial drop in the emission intensity seen clearly for the slower kinetics, as will be discussed later on. It is in this region that the current understanding lacks concrete experimental support. The inset in Figure 1 shows the XANES spectra for the 2 mM solution collected at the times indicated. Note that the absorption edge steps for these spectra can be read in the figure caption and give exactly the same kinetic pattern as the integrated fluorescence intensity.

The XAS spectrum at time "zero" (curve a in Figure 1) displays a strong, narrow peak that is characteristic of a gold

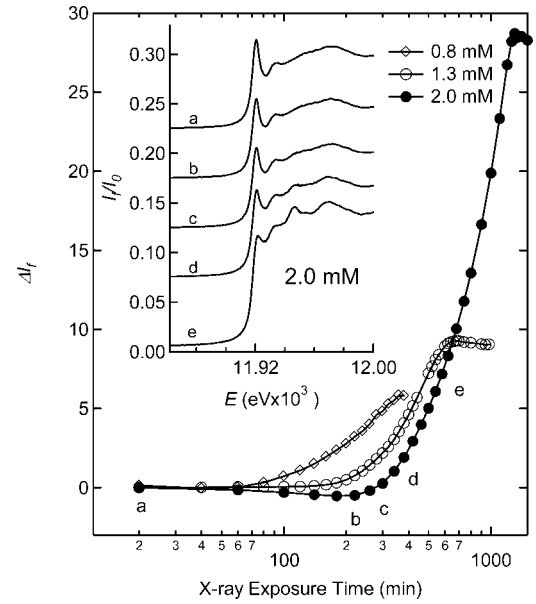

Figure 1. Kinetics of X-ray induced Au reduction from solution illustrated by the measured Au L_3 fluorescence vs time. The inset shows the XANES spectra as a function of X-ray exposure time for 2 mM solutions as examples: (a) 0 min, $\Delta\mu = 0.079$; (b) 220 min, $\Delta\mu = 0.076$; (c) 300 min, $\Delta\mu = 0.080$; (d) 420 min, $\Delta\mu = 0.095$; (e) 680 min, $\Delta\mu = 0.137$; where $\Delta\mu$ is the absorption edge step.

triple oxidation state ($5d^8$) for halide compounds or Au_2O_3 and is assigned to a $2p_{3/2} \rightarrow 5d$ transition.[23,24] The intensity and position of this peak varies with the ion charge and the electron affinity of the ligand (influenced by both initial and final state effects).[23,25] It is used as a benchmark for the Au^{3+} state here. The absorption edge defined by the deflection point of the rising step is found at ~0.5 eV below that of the gold metal, which is somewhat smaller than the value for Au_2O_3.[24] As the X-ray dose increases this peak attenuates and disappears, and a distinct structure that is typical of the gold metal appears. The data are thus compounded, at least with these two components.

To decompose the spectra, the "zero" dose spectrum is combined either with an AuI or a gold metal spectrum to fit the sample spectra using a linear combination analysis (LCA) routine.[26] No shifts in spectral energy are allowed because all the spectra are energy referenced to that of gold metal that is simultaneously measured. The spectra can be reasonably fitted in both cases with similar weighting factors. However, analysis of the fitting merits indicates that the fits that involve the AuI spectrum are better. The merit is defined by eq 1,[26]

$$\sum_i (\text{data} - \text{fit})_i^2 / \sum_i \text{data}_i^2 \qquad (1)$$

which ranges from 3.87×10^{-3} to 7.2×10^{-3} for the 2.0 mM data in the first region. Figure 2 shows the differential merits obtained by subtracting the fitting merits for $HAuCl_4$ and Au from those for $HAuCl_4$ and AuI, as model compounds, respectively. The quick rises indicate that gold precipitation starts to dominate the system at the onset of the second region, whereas the general downward trends in the first region suggest that the monovalent Au state is preferred. Poor data quality for 1.3 mM is simply due to lower concentration, and the results are even worse for 0.8 mM (not shown). Fits using all three compounds, that is, $HAuCl_4$, Au, and AuI, in the LCA routine were also carried out. The results are shown in Figure 3, where the weights for three components are presented as a function of time. It is seen that the percentage of Au does not rise up to

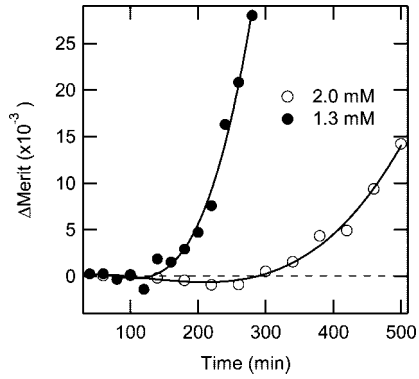

Figure 2. Linear combination simulation merit analysis results for two solutions. The analyses use the $HAuCl_4$ spectrum and either the AuI or the Au spectrum. ΔMerit = Merit(1) − Merit(2), (1) $HAuCl_4$/AuI and (2) $HAuCl_4$/Au.

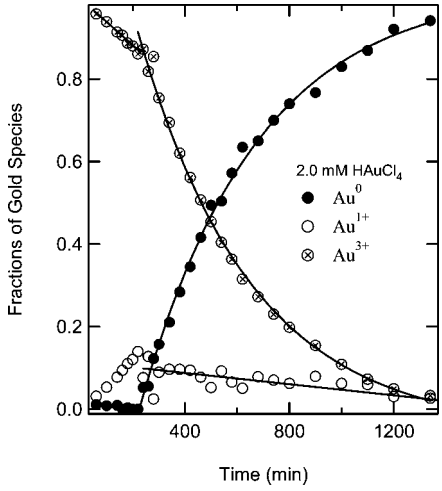

Figure 3. Fractions of three gold species as a function of time, obtained by the LCA analysis using three components, $HAuCl_4$, Au, and AuI.

any statistic significance in the first region. These results are consistent with that described in Figure 2. Therefore, no direct conversion of Au^{3+} to Au^0 is observed; rather, a conversion to the Au^{1+}state is strongly indicated. From the two-component analysis it is possible to obtain the difference spectra: $\Delta S_t = S_t - wS_{t=0}$, where w is the weight of the "zero" dose spectrum. Note that only the w factor for $HAlCl_4$ is used in the calculation.

Figure 4 shows ΔS_t for the 2 mM solution compared to the spectra of AuI and Au. The inset plots the absorption edge positions of these ΔS_t values, relative to that of gold metal, versus time compared to those of $HAuCl_4$ and AuI. Despite the noise, the difference spectra in the first region remarkably reproduce the features associated with the monovalent gold, in particular, the edge feature (d^{10}). Therefore it can be concluded with great certainty that, prior to gold precipitation in these solutions, the Au^{1+} state forms as an intermediate under X-ray illumination. It increases to ~12% at the juncture between the first and second regions (see Figure 3), strictly following the zero-order kinetics $C - C_0 = -kt$ ($k_{2mM} = 10^{-5}$ s^{-1}), typical for a photochemical reaction. This explicitly shows that the Au^{3+} complexes are reduced to the Au^{1+} ones as one of the intermediate steps and validates the reaction $AuCl_4^- + e_{aq}^- \rightarrow AuCl_2^- + 2Cl^-$.

The changes in the first region are also quantifiable by the changes in the local coordination, N, because the Fourier transforms of the EXAFS spectra (not shown here) can be modeled well by $N = wN_{Au^{3+}} + (1 - w)N_{Au^{1+}}$ ($N_{Au^{3+}} = 4$ and

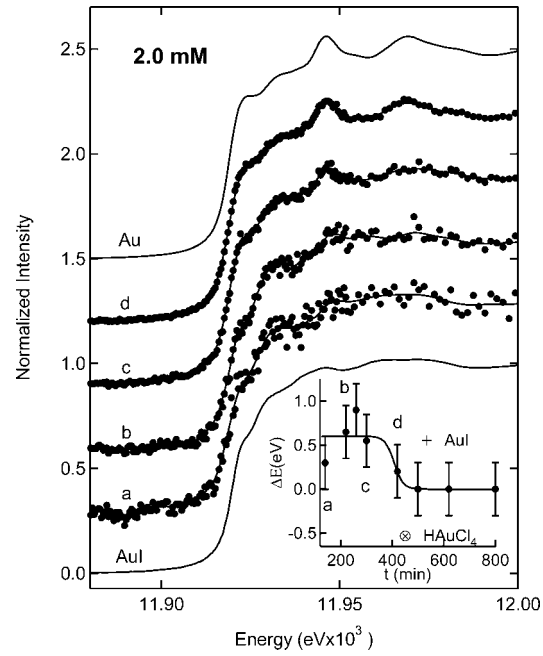

Figure 4. Difference spectra from the measurements at various exposure times for the 2 mM solution are compared with the Au and AuI spectra: (a) 140 min, (b) 220 min, (c) 300 min, and (d) 420 min. The inset is the absorption edge shift versus time relative to the Au^0 L_3 edge, determined from the difference spectra and compared with the Au L_3 edges of AuI (cross) and $HAuCl_4$ (cross and circle).

2). In the second region, the metallic XANES structure becomes distinct, which marks the metal precipitation in the solutions (see the inset in Figure 1).

B. Morphological Changes in the Aqueous Solutions under X-ray Irradiation. The step towards metal precipitation, however, may involve more than chemical change. Figure 5 displays in the top panel for the 2 mM solution, the Au L_3 X-ray emission increase ΔI_f, and small angle scattering intensity I_{saxs} versus X-ray exposure time. In the experiments, a 30-second SAXS exposure is executed before each 20 min Au L_3 emission measurement. The integrated data are presented. The inset displays the SAXS profiles as a function of time. For a diluted, spherical particulate system the scattering intensity is proportional to the difference square of the electron densities of the particulate and matrix: $I(q)\ \alpha\delta\rho_e^2$, where $q = 4\pi \sin\theta/\lambda$. The absolute intensity, $I_{abs}(q) = [I(q) - I_m(q)e^{-\mu x}]/[\mu x I_0 e^{-\mu_m x}]$, where m denotes matrix, that is , H_2O + Kapton in this case. The system is essentially noninteractive. Unlike the emission intensity, the scattering intensity increases monotonically, and the increase rate starts to top off before the onset of the third region. In the first region alone, the scattering intensity increased by ~37%, whereas the emission intensity remained unchanged or decreased somewhat. These results unequivocally show that under X-ray irradiation the gold complexes rearrange, likely aggregate, resulting in the increased density contrast $\delta\rho$ and, thus, increased I_{saxs}, even before the occurrence of any metal precipitations. The reason for the initial drop in ΔI_f could be complex. The effect is obvious for the 2 mM solution due to the slower kinetics (seen better in Figure 1). It may result from some of the aggregates moving out of the beam in the first region. However, this is inconsistent with what happens in the second region, as will be discussed below, where the gold clearly accumulates. Another likely cause may be the increased intergold-complex shadowing of the exiting Au L_3 emission photons as they aggregate. This assertion seems to better reconcile with the SAXS data. Of course, it is also possible for

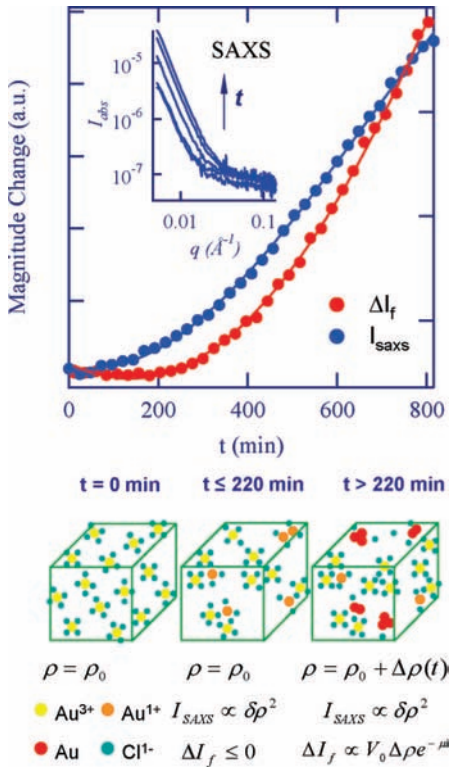

Figure 5. Top panel: the circular- and q-integrated SAXS intensity and the L_3 emission intensity vs X-ray exposure time. The inset shows the circular-integrated SAXS data. Bottom panel: a cartoon illustration of the evolution of the solution under X-ray illumination and corresponding mathematic description.

both of these mechanisms to coexist. Therefore, in addition to the reaction, $Au^{3+} + 2e^-_{aq} \rightarrow Au^{1+}$, a process, such as $nAuCl_2^{1-} \rightarrow [AuCl_2^{1-}]_n$ and/or $nAuCl_4^{1-} \rightarrow [AuCl_4^{1-}]_n$, proceeds simultaneously.

The Au L_3 emission intensity is largely determined by the mass. Therefore, the rise in the emission intensity in the second region indicates an accumulation of gold atoms in the X-ray beam path, once metal precipitation occurs. The rise in the X-ray scattering intensity in this region is thus weighted by metal precipitation and increased gold density. The top-off of the scattering intensity before ΔI_f is likely due to the bulk texture formation, and indeed, the gold deposition on the Kapton window starts to be visible. The bottom panel in Figure 5 gives a cartoon illustration of the evolution in the solution.

Figure 6 shows the Fourier transforms of the difference EXAFS spectra, calculated in a way described above, as a function of X-ray exposure time, which are compared to that of the gold foil. It is seen that at 300 min the metallic feature dominates the spectrum and increases as a function of time. At 800 min, it is essentially undistinguishable from that of bulk. The bulk gold has a close-packed cubic structure, and each atom is neighbored by 12 others. For small gold particles N is smaller than 12. Assuming a globular shape for the produced gold particles, it is possible to appreciate the particle sizes using $\eta = N/N_{bulk}$,[27] which can be obtained from the data in Figure 6. It is estimated that the particle size is ~0.5 nm ($\eta = 0.55$) at 300 min, ~1.0 nm ($\eta = 0.83$) at 420 min, and >8.0 nm ($\eta = 1$) at 800 min.

C. Gold Nanoparticle Generation Kinetics and Mechanism. The second region shows a rate that is nearly independent of the concentration: $\Delta I_f/\Delta t \approx$ constant. This may indicate that the diffusion is not a limiting factor for the process, likely due

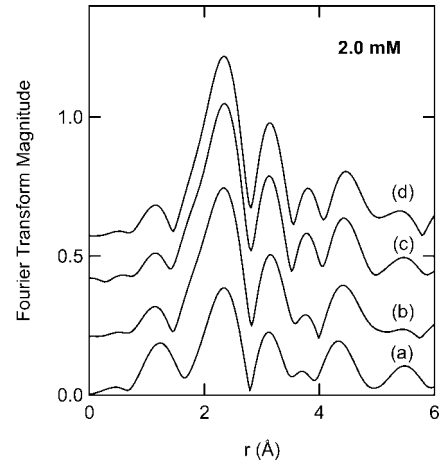

Figure 6. Fourier transforms of the differential EXAFS spectra measured for the 2.0 mM solution at (a) 300 min, (b) 420 min, and (c) 800 min, compared to the gold foil (d).

to the low concentrations. In fact, it will be misleading to use the emission data to describe the reaction kinetics because they mostly reflect the gold accumulation in the X-ray beam path. The true kinetics can only be revealed by separating the reactant and products. This was accomplished by the LCA analysis using all three gold species, as mentioned above and presented in Figure 3 for the 2.0 mM solution. The reaction is a priori first order for Au^{3+} and Au, that is , $C_{Au^{3+}} = C_0 e^{-kt}$ and $C_{Au} = C_0(1 - e^{-kt})$ with $k \approx 4 \times 10^{-5}$ sec^{-1} and that the fraction of Au^{1+} decreases linearly from ~12%. The intrinsic relation between Au^{3+} and Au may imply that the reduction is perpetuated by other mechanisms as well besides photochemical.

The pH measurements at the juncture between the first and second regions indicate that the solution acidity departed from the initial pH value of 2.8 towards 4 for the 2 mM solution. This is consistent with the recent report by C−H Wang et al. who used a polychromatic X-ray beam.[28] Therefore, the hydrolysis equilibrium has been changed under X-ray irradiation. It is also noticed that bubbles slowly form near the solution top as X-ray exposure proceeds. One of the reactions leading to the pH change could be $e^-_{aq} + H \rightarrow H_2 + OH^-$.[22] The excessive Cl^- ions may exit as Cl_2. There is an inverse linear relationship between the onsets of the metal precipitation versus the pH values (see Figure 1). For the given X-ray dosing rate, it takes longer for gold to precipitate in a more acidic solution. Experiments with a buffered 2 mM solution show that the process in the first region is drastically slowed down. This suggests that the solution pH conditions play an influential role in the eventual metal precipitation. At pH ≥ 4, the $AuCl_4^-$ and/or $AuCl_4^-$complexes are no longer stable. The experiments with pH-adjusted $HAuCl_4$ solutions (adding NaOH) show an immediate metal precipitation under X-ray irradiation for pH > 7. The XANES spectra (not shown) bear the clear signature of the substitution of Cl^- by OH^-,[24] being a reductant itself. It is also likely that hydrate electrons are more efficient in an alkaline solution.[22]

Another possible influence is from the formed Au particles. The previous works concluded that the reduction of Au^{3+} in the presence of pre-formed particles is catalytic in nature, which may lead to direct reduction of Au^{3+} to Au through, say, a surface mediated mechanism.[29] It is shown that the reduction continues after irradiation.[6,12]

The driving force for gold ions to migrate into the X-ray beam path is not clear. Fick's first law may play a role for $AuCl_4^-$ to

migrate into the beam, because these anions are consumed by reduction in the beam and a concentration gradient may exist. We also speculate that under high energy X-ray irradiation a charge imbalance in the system may be created because the generated electrons are more mobile than the ions. With this argument, the X-ray illuminated volume should be charged more positively than the nonilluminated volume. The complexes such as $AuCl_4^-$ will be driven towards the illuminated area through the Columbic interaction and will thus accumulate. The gold deposition on the Kapton windows is also believed to be related to the X-ray induced charge effect.[30]

Conclusions

The X-ray induced gold reduction process is essentially similar to those induced by UV light or γ-rays. The combination of X-ray absorption spectroscopy and small angle X-ray scattering has provided unprecedented details about chemical and morphological changes in the solutions under irradiation. It is a powerful approach for studies of liquid or colloidal systems in real time. Prior to metal precipitation, the intermediate state, also observed by other techniques,[4,9–11] is unambiguously determined for the first time to be the reduction of Au^{3+} to Au^{1+}, whose kinetics is strictly of the zeroth order. The morphological changes occur simultaneously in the solutions, that is, the gold complexes rearrange and aggregate, as unequivocally observed by the correlated changes in the Au L_3 emission and small angle scattering intensities. The experimental evidence indicates that the eventual metal precipitation is strongly influenced by the changing solution acidity under X-ray irradiation.

Acknowledgment. DND-CAT is supported by E.I. DuPont de Nemours & Co., The Dow Chemical Company, and State of Illinois funding to Northwestern University. The Advanced Photon Source and The Center for Nanoscale Materials at Argonne National Laboratory are supported by the U. S. Department of Energy, Office of Science, Office of Basic Energy Sciences, under Contract No. DE-AC02-06CH11357.

Supporting Information Available: Two figures are provided that show the raw XANES spectra and the normalized XANES spectra, as a function of time. The detailed description of the integrated fluorescence intensity is also given. This information is available free of charge via the Internet at http://pubs.acs.org.

References and Notes

(1) Burda, C.; Chen, X.; Narayanan, R.; El-Sayed, M. A. *Chem. Rev.* **2005**, *105*, 1025.
(2) *Nanoscale Materials in Chemistry*, Klabunde, K. J., Ed.; John Wiley & Sons: New York, 2001.
(3) Paclawski, K.; Fitzner, K. *Metall. Mater. Trans.* **2006**, *B37*, 703.
(4) Skibsted, L. H. *Adv. Inorg. Bioinor. Mech.* **1986**, *4*, 137.
(5) Zhao, C.; Qu, S.; Zhu, C. *J. Mater. Res.* **2003**, *18*, 1710.
(6) (a) Eustis, S.; El-Sayed, M. A. *J. Phys. Chem.* **2006**, *B110*, 14014. (b) Eustis, S.; Hsu, H.-Y.; El-Sayed, M. A *abid* **2005**, *109*, 4811.
(7) Murphy, C. J.; Jana, N. R. *Adv. Mater.* **2002**, *14*, 80.
(8) Chen, S.; Wang, Z. L.; Ballato, J.; Foulger, S. H.; Crroll, D. L. *J. Am. Chem. Soc.* **2003**, *125*, 16186.
(9) Bjerrum, N. *Bull. Soc. Chim. Belges* **1948**, *57*, 432.
(10) (a) Lingane, J. J. *J. Electroanal. Chem.* **1958**, *19*, 394. (b) Lingane, J. J *abid.* **1962**, *4*, 332.
(11) Henglein, A. *Langmuir* **1999**, *15*, 6738.
(12) Gachard, E.; Remita, H.; Khatouri, J.; Keita, B.; Nadjo, L.; Belloni, J. *New J. Chem.* **1998**, *22*, 1257.
(13) Pan, P.; Wood, S. A. *Geochim. Cosmochim. Acta* **1991**, *26*, 671.
(14) Murphy, P. J.; Stevens, G.; LaGrange, M. S. *Geochi. Cosmochim. Acta* **2000**, *64*, 479.
(15) Baily, E. H.; Scofield, P. F.; Mosselmans, J. F. *Proceedings of the 7th Annual V. M. Goldschmidt Conference*, Lunar and Planetary Institute, Houston, TX, 1997; Vol. 921; p 2264.
(16) Koutek, M. E.; Mason, W. R. *Inorg. Chem.* **1980**, *19*, 648.
(17) Kunkely, H.; Vogler, A. *Inorg. Chem.* **1992**, *31*, 4539.
(18) Sayers, D. E.; Stern, E. A.; Lytle, F. W. *Phys. Rev. Lett.* **1971**, *27*, 1204.
(19) Guinier, A.; Fournet, G. *Small-Angle Scattering of X-rays*; Wiley & Sons: New York, 1955.
(20) Henglein, A. *Langmuir,* **1998**, *14*, 7393.
(21) Ghosh-Mazumdar, A. S.; Hart, E. J. *Adv. Chem. Ser.* **1968**, *81*, 193.
(22) Hart, E. J. *Science* **1964**, *146*, 19.
(23) Choy, J.-H.; Kim, Y.-I. *J. Phys. Chem.* **2003**, *B107*, 3348.
(24) Berrodier, I.; Farges, F.; Benedetti, M.; Winterer, M.; Brown, M. G., Jr.; Deveughèle, M. *Geochim. Cosmochim. Acta* **2004**, *68* (14), 3019.
(25) Brown, N. M. D.; McMonagle, J. B.; Greaves, G. N. *J. Chem. Soc., Faraday Trans. I* **1984**, *80*, 589.
(26) Ravel, B. The Consortium for Advanced Radiation Sources;http://cars9.uchicago.edu/~ravel/software/, 2005.
(27) Greegor, R. B.; Lytle, F. W. *J. Catal.* **1980**, *63*, 476.
(28) Wang, C.-H.; Hau, T.-E.; Chien, C.-C.; et al. *Mater. Chem. Phys.* **2007**, *106*, 323.
(29) Henglein, A. *Langmuir* **1998**, *14*, 7393.
(30) Ma, Q.; Moldovan, N.; Mancini, D. C.; Rosenberg, R. A. *Appl. Phys. Lett.* **2000**, *76*, 2015.

JP7104852